



Trans. Nonferrous Met. Soc. China 35(2025) 538-551

Transactions of Nonferrous Metals Society of China

www.tnmsc.cn



Corrosion behavior and life prediction of SAC305 solder joints in PVC fire smoke

Meng-ke ZHAO, Jian-rui FENG, Qian LI, Shou-xiang LU, Jin LIN

State Key Laboratory of Fire Science, University of Science and Technology of China, Hefei 230026, China

Received 6 July 2023; accepted 29 March 2024

Abstract: The corrosion behavior and life of Sn-3.0Ag-0.5Cu solder joints were investigated through fire smoke exposure experiments within the temperature range of 45-80 °C. The nonlinear Wiener process and Arrhenius equation were used to establish the probability distribution function and prediction model of the solder joint's average life and individual remaining useful life. The results indicate that solder joint resistance shows a nonlinear growth trend with time increasing. After 24 h, the solder joint transforms from spherical to rose-like shapes. Higher temperatures accelerate solder joint failure, and the relationship between failure time and temperature conforms to the Arrhenius equation. The predicted life of the model is in good agreement with experimental results, demonstrating the effectiveness and accuracy of the model.

Key words: solder joints; fire smoke; corrosion behavior; electrical performance degradation; life prediction model

1 Introduction

As the I/O end of the circuit, the solder joints are the critical part of the electromechanical connection and the key to the reliability of electronic equipment [1]. In the past, the primary solder alloy used was the Sn-Pb. Due to the toxicity limitation of Pb, the Sn-Ag-Cu (SAC) lead-free solder alloy has been extensively employed as a substitute for lead-based solder. The most widely used alloy is Sn-3.0Ag-0.5Cu (SAC305) [2,3]. However, lead-free solder alloys are more susceptible to corrosion than Su-Pb solder alloy [4]. The corrosion of solder alloy will affect the regular operation of electronic equipment and even lead to unpredictable consequences [5].

In the electronic processing industry, many combustible materials will bring serious fire hazards, resulting in frequent fire accidents [6]. For

instance, on March 19, 2021, a devastating fire broke out at Renesas Naka Factory, resulting in substantial economic damages. The damage caused by fire is commonly categorized into thermal damage and non-thermal damage. Non-thermal damage has received extensive attention due to its strong propagation and wide-ranging effects. Especially in the electronic processing industry, there is a significant presence of wires and cables composed of polyvinyl chloride (PVC) material. The smoke generated from PVC combustion exhibits severe corrosiveness, especially towards lead-free solder alloy [7–9]. Therefore, it is imperative to investigate the corrosion behavior and degradation law of solder joints in fire smoke environments and predict the remaining useful life (RUL) of solder joints after corrosion. Accurate life prediction can provide scientific guidance for formulating post-disaster electronic equipment rescue strategies.

Currently, there are few studies on the corrosion behavior of lead-free solders in fire smoke environments. Most studies have focused on the corrosion behavior of lead-free solder in marine atmospheric environments. Salt spray tests or NaCl thin electrolyte layers are often employed to simulate the marine atmospheric environment. The results indicate that the thickness of the electrolyte influence the solder's can corrosion mechanism [10,11]. Under a thicker electrolyte layer, the cathodic process primarily dominated by oxygen diffusion is the primary corrosion mechanism. In contrast, anodic dissolution is more likely to control corrosion under a thinner electrolyte layer. Additionally, some researchers have investigated the influence of the composition of solder alloys on the corrosion behavior in a marine environment. It has been found that increasing the silver content in SAC solder reduces the corrosion current density, thereby enhancing the corrosion resistance of the alloy [12]. Furthermore, the cooling rate [13] and other element contents [14,15] during preparation of Sn-based solder alloys can influence the morphology of intermetallic compounds [16], thereby affecting the corrosion behavior and life of solder joints [17].

The research on the life prediction of corroded lead-free solder is of great significance for ensuring the long-term reliability of electronic devices in harsh environments. Previous studies indicated that solder joints are more susceptible to corrosion under the same environment than solder alloys [18,19]. The presence of copper solder pads can lead to galvanic corrosion, thereby accelerating the corrosion of solder joints and reducing the life of electronic devices [20]. Prediction methods based on traditional statistical models, such as the lognormal distribution model [21] and Weibull distribution model [22,23], have been widely used solder joints' evaluate reliability characteristic life under salt spray corrosion. However, the traditional method requires a large amount of failure time (FT) data [24]. It can only predict the overall life of the electronic devices, but not the RUL of individual devices. Additionally, temperature can significantly accelerate the corrosion process of solder alloys [25]. Especially in the fire smoke environment, temperature variations are more pronounced compared to normal operating conditions, posing a severe threat to the reliability of solder joints. Therefore, there is an urgent need to investigate the RUL of solder joints at different temperatures in the fire smoke environment.

Therefore, this work aims to investigate the impact of temperature on the electrical performance and predict the life of SAC305 solder joints in the fire smoke environment. The main contributions of this work include three aspects: (1) The corrosion behavior of solder joints at different temperatures in the fire smoke environment is studied through accelerated degradation test (ADT); (2) Real-time data on the degradation of solder joints are obtained through electrical performance measurements, revealing the characteristics of the solder joint degradation path; (3) A real-time prediction framework for the RUL of solder joints is proposed and validated through experimental data. This work guides damage assessment of electronic devices and formulation of emergency rescue strategies after fire.

2 Experimental

2.1 Materials and components

In this study, ball grid array (BGA) bare chips provided by Amkor Corporation were employed to observe the surface corrosion morphology. The BGA was assembled onto printed circuit boards to create board-level components, which were manufactured by Jingbang Electronics Co., Ltd. These board-level components were utilized for real-time testing of electrical performance degradation. The electrical connection path structure between solder joints is shown in Fig. 1. The board-level components were rinsed using deionized water, followed by ultrasonic cleaning with anhydrous

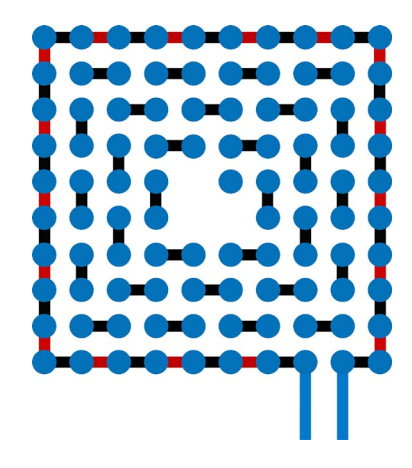


Fig. 1 Schematic diagram of solder joint connection

ethanol, and dried with compressed air. This process was carried out to obtain a clean surface of board-level components, avoiding interference from other substances on the electrical performance measurement.

2.2 Experimental design

The smoke corrosion system simulated a fire smoke environment at different temperatures. (15±0.1) g PVC powders were heated using a tubular furnace. The generated smoke was transported into the exposure chamber through insulated PVC pipes. The board-level components were exposed to the smoke for 3 h after the smoke introduction. Subsequently, the constant temperature and humidity system was activated to maintain the exposure chamber at a constant temperature and humidity level until the board-level components failed. Each experimental condition times. repeated three Moreover, experiment included three board-level components of the same type.

The rated temperature range of electronic devices varied according to application scenarios, ranging from -5 to 45 °C. Therefore, the temperature stress of the electronic equipment was assumed to be 45 °C in the normal operating condition. The ADT was conducted under disparate temperatures of 45, 50, 55, 65, and 80 °C. The relative humidity inside the chamber was maintained at 85% throughout the exposure.

2.3 Characterization method

To better observe the corrosion behavior of solder joints in fire smoke, scanning electron microscope (SEM, GeminiSEM 500) was employed to examine the microstructure of the solder joints

before corrosion, as well as at 3, 24 and 48 h after corrosion. Furthermore, to better understand the corrosion behavior of various board-level components, the resistance changes rate (RCR, ΔR) was employed as a performance characterization parameter to evaluate their health status, which was calculated using Eq. (1). The failure threshold was defined as a 20% increase in the resistance of board-level components compared to their initial values.

$$\Delta R(t_i) = \frac{R(t_i) - R(t_0)}{R(t_0)} \tag{1}$$

where $R(t_0)$ is the initial resistance at the moment of t_0 , Ω ; $R(t_i)$ is the resistance at the moment of t_i , Ω , and $\Delta R(t_i)$ is the RCR at the moment of t_i , %.

2.4 Life prediction method

2.4.1 Life prediction model

In practical engineering applications, the corrosion resistance of solder joints is of vital importance for the safety and reliability of electronic devices. Therefore, it is necessary to analyze the life of solder joints after exposure to fire smoke. The Wiener process, Y(t), was used to describe the corrosion degradation behavior of solder joints [26].

$$Y(t) = \mu \cdot \tau(t; \beta) + \sigma \cdot B(\tau(t; \beta)) \tag{2}$$

where μ is the drift coefficient, representing the difference between units caused by manufacturing or the external environment; the diffusion coefficient σ represents the uncertainty related to time in the product degradation process; $B(\cdot)$ is the standard Brownian motion; $\tau(t; \beta) = t^{\beta}$ is a monotone continuous nonlinear function of time t. When $\beta \neq 1$,

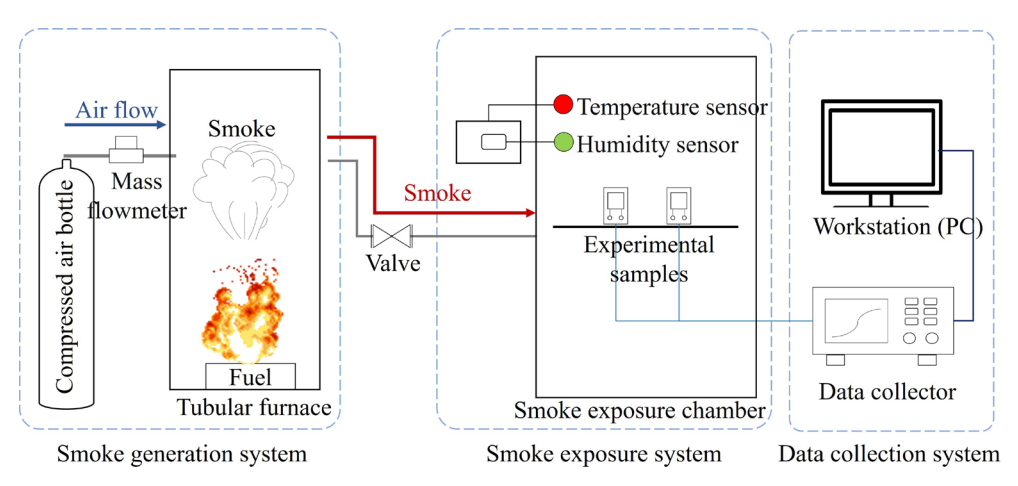


Fig. 2 Schematic diagram of smoke corrosion system

it is a convex or concave function, which can be applied to most degradation processes [27].

Assuming that the Arrhenius equation can effectively describe the relationship between temperature and life [28], a model is established using the Arrhenius equation to depict the relationship between model parameters and temperature.

$$\mu(T) = a_1 e^{-c_1/T} \tag{3}$$

$$\sigma(T) = a_2 e^{-0.5c_1/T} \tag{4}$$

where T represents temperature (°C); a_1 , a_2 and c_1 are the undetermined constants.

Since the Wiener process follows the normal distribution, the accelerated degradation model can be expressed as

$$Y(t; T) \sim N\left(a_1 e^{-c_1/T} \tau(t; \beta), a_2^2 e^{-c_1/T} \tau(t; \beta)\right)$$
 (5)

The failure threshold of the product is assumed to be D. The product's life can be defined as the time when the degradation process first reaches the failure threshold, which is called the first arrival time γ .

$$\gamma = \inf \left\{ t \mid Y(t) \ge D \right\} \tag{6}$$

Due to the randomness of the degradation process, the life γ is a random variable. $f_{\gamma}(t)$ and $F_{\gamma}(t)$ are its corresponding probability density function (PDF) and cumulative distribution function (CDF), respectively. Based on the definition of first arrival time, the CDF of the product follows the inverse Gaussian distribution [29].

$$f_{\gamma}(t;\mu,\sigma,D) = \frac{D}{\sqrt{2\pi\sigma^{2}\tau^{3}(t;\beta)}} \exp\left[-\frac{\left(D - \mu\tau(t;\beta)\right)^{2}}{2\sigma^{2}\tau(t;\beta)}\right] \frac{d\tau(t;\beta)}{dt}$$
(7)

$$F_{\gamma}(t;\mu,\sigma,D) = \Phi\left(\frac{\mu\tau(t;\beta) - D}{\sqrt{\sigma^{2}\tau(t;\beta)}}\right) + \exp\left(\frac{2\mu D}{\sigma^{2}}\right)\Phi\left(-\frac{\mu\tau(t;\beta) + D}{\sqrt{\sigma^{2}\tau(t;\beta)}}\right)$$
(8)

where $\Phi(\cdot)$ is CDF of the standard normal distribution.

Therefore, the average life ($\overline{\xi}$) prediction model of board-level components after smoke

corrosion is deduced as

$$\overline{\xi} = D/(\beta\mu) \tag{9}$$

In accordance with the accelerated degradation model in Eq. (5), the log-likelihood function is established based on the PDF of normal distribution.

$$L(\mu, \sigma, \beta) = \prod_{k=1}^{M} \prod_{j=1}^{N_k} \frac{\exp\left[-\frac{(\Delta y_{ijk} - a_1 e^{-c_1/T_k} \Delta \tau_{ijk})^2}{2a_2^2 e^{-c_1/T_k} \Delta \tau_{ijk}}\right]}{\sqrt{2\pi a_2^2 e^{-c_1/T_k} \Delta \tau_{ijk}}}$$
(10)

where $\Delta y_{ijk} = y_{ijk} - y_{(i-1)jk}$ represents the increment of degradation, and $\Delta \tau_{ijk} = \Delta \tau_{ijk} - \Delta \tau_{(i-1)jk}$ denotes the increment of time. Among them, $i=1, 2, \dots, H_{jk}, j=1, 2, \dots, N_k$, and $k=1, 2, \dots, M$. H_{jk} is the total measurement time of each product under each accelerating temperature stress. N_k is the total number of components under each accelerating temperature stress. M is the total number of accelerating temperature stress.

MATLAB software and the maximum likelihood estimation (MLE) method are devoted to the model parameter estimation. The estimate of parameters $(\hat{\mu}, \hat{\sigma})$ will be acquired. Consequently, the overall average life of the products is calculated based on the average life prediction model (Eq. (9)). 2.4.2 Adaptive update of parameters

The products exhibit inherent time variability during the degradation process. RUL represents the real-time changes in product life during the degradation process. RUL refers to the time interval from the current state to the first failure. Supposing D' is the amount of degradation corresponding to RUL, then when the value of degradation progresses Y(t) < D, D' = D - Y(t). The PDF and CDF of RUL are expressed as

$$f_{\text{RUL}}(t; \mu, \sigma, D') = \frac{D'}{\sqrt{2\pi\sigma^2 t^{3\beta}}} \exp\left[-\frac{\left(D' - \mu t^{\beta}\right)^2}{2\sigma^2 t^{\beta}}\right] \beta t^{\beta - 1}$$
(11)
$$F_{\text{RUL}}(t; \mu, \sigma, D') = \Phi\left(\frac{D' - \mu t^{\beta}}{\sqrt{\sigma^2 t^{\beta}}}\right) - \exp\left(\frac{2\mu D'}{\sigma^2}\right) \Phi\left(-\frac{D' + \mu t^{\beta}}{\sqrt{\sigma^2 t^{\beta}}}\right)$$
(12)

Based on the Eqs. (11) and (12), the RUL prediction model is indicated as Eq. (13).

$$\overline{\xi}_{\text{RUL}} = D'/(\beta\mu) \tag{13}$$

Additionally, even for the same type of products, there are differences in the RUL among individual products, referred to as individual variations. Traditional prediction methods can only forecast the average life of board-level components and are incapable of accurately predicting the individual life of each distinct board-level component [30]. Therefore, the parameters μ and σ are taken as random parameters and assumed to be uncorrelated to distinguish individual variations better.

The Bayesian method based on Markov Chain Monte Carlo (MCMC) is employed to estimate and update random parameters. We assume that the random parameters follow a non-conjugate prior distribution, meaning the posterior distribution of the parameters is not within the same distribution family as the prior. The prior distribution of the parameters is based on the estimated values obtained in Section 2.4.2. The parameter estimates at different temperatures are transformed into estimates at a fixed temperature using Eq. (14). The detailed derivation process is presented in the Supporting Information. Then, the Anderson-Darling (AD) test determines the optimal fitting distribution type for model parameters. A smaller AD statistic indicates a better fit between the data and the selected distribution.

$$A_{k,l} = \left(\frac{\mu_k}{\mu_l}\right)^{1/\beta} = \left(\frac{\sigma_k^2}{\sigma_l^2}\right)^{1/\beta} = \left[\exp\left(c_1\left(\frac{1}{T_l} - \frac{1}{T_k}\right)\right)\right]^{1/\beta}$$
(14)

where $A_{k,l}$ denotes the accelerated factor, which reflects the acceleration effect of a certain acceleration stress level in the ADT.

Furthermore, the posterior PDF of random parameters can be deduced by Bayesian method. Let $Y=[y(t_1), y(t_2), ..., y(t_i)]$ be the field monitoring degradation data of the same board-level component under operating temperature stress at time t_i .

$$f(\mu, \sigma^{2} | \Delta Y) = \frac{L(\Delta Y | \mu, \sigma^{2}) \cdot f(\mu, \sigma^{2})}{\int_{-\infty}^{+\infty} \int_{-\infty}^{+\infty} L(\Delta Y | \mu, \sigma^{2}) \cdot f(\mu, \sigma^{2}) d\mu d\sigma^{2}}$$
(15)

where $L(\Delta Y|\mu, \sigma^2)$ is the likelihood function. The prior PDF $f(\mu, \sigma^2)$ of random parameters is $f(\mu, \sigma^2)=f(\mu)\cdot f(\sigma^2)$. The posterior PDF of $\mu|\Delta Y$ and

 $\sigma^2 | \Delta Y$ can be indicated as

$$f(\mu \mid \Delta Y) \propto L(\Delta Y \mid \mu, \sigma^2) \cdot f(\mu)$$
 (16)

$$f(\sigma^2 \mid \Delta Y) \propto L(\Delta Y \mid \mu, \sigma^2) \cdot f(\sigma^2)$$
 (17)

Subsequently, the expectations can be obtained through the posterior distribution of model parameters $\mu | \Delta Y$ and $\sigma^2 | \Delta Y$.

The posterior distribution of parameters is fitted using Gibbs sampling to address the challenge of obtaining posterior expectations of parameters. The Gibbs sampling method is primarily employed when the joint distribution of multivariate variables is unclear or difficult to sample directly, but the conditional distribution of each variable is known and can be easily sampled. Therefore, the Gibbs sampling method is applied to estimating the posterior values of the parameters, as illustrated in Fig. 3. The parameter estimation is obtained by averaging all converged values between different initial values. Among them, the final average value is performed on the vector of parameter values generated over all iterations after convergence.

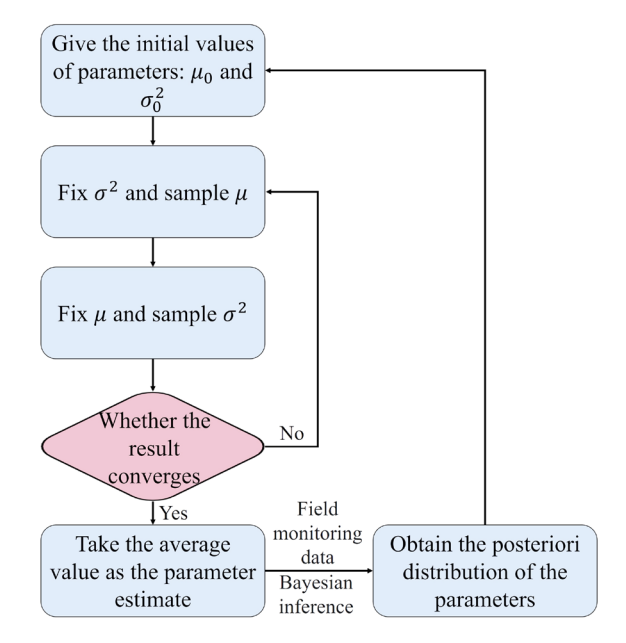


Fig. 3 Flow chart of Gibbs sampling method

In summary, we can derive various parameter estimates based on the obtained degradation data of solder joints at different temperatures. These estimated values are transformed into unified estimates at a consistent temperature using an acceleration factor. The AD test is employed to select the best-fitting distribution for the random parameters, allowing individual variations to be

reflected through the randomness of the parameters. Subsequently, the Gibbs sampling is utilized for parameter estimation. Bayesian method is iteratively applied to updating the random parameters with individual variations, enabling real-time prediction of RUL for different board-level components. The basic process of RUL prediction is illustrated in Fig. 4.

3 Results and discussion

3.1 Corrosion behavior

Solder joints were exposed to the fire smoke environment for 0, 3, 24 and 48 h, and the surface corrosion morphology is shown in Fig. 5. Additionally, to better compare the size characteristics of corrosion morphology at different time, Nano Measurer software was used to measure the diameter of the solder joints. The red line in Fig. 5(a) indicates the measurement location. As depicted in Fig. 5(a), the initial morphology of the solder joint is spherical, with an initial diameter of 264.6 µm. After 3 h of exposure, the solder joints exhibit evident corrosion, as shown in Fig. 5(c). The solder joints remain spherical, with the diameter increasing to 276.8 µm. After magnification, it is found that the microstructure of the solder joint transforms from compact structures to prickly structures. There are a lot of corrosion pits and thin sheet corrosion products on the surface of the solder joint, and the average thickness is about 0.3 µm (for 10 corrosion products structures). With increasing exposure time, at 24 h, the corrosion products on the solder joint transform into loose, thick plate-like structures with an average thickness of 6.6 µm. The diameter of solder joints significantly increases to 384.8 µm, evolving from its initial spherical shape to a blooming rose pattern. At 48 h, the diameter of solder joints is 358.0 µm. The average thickness of the plate-like corrosion products is 4.3 µm, showing no significant change compared to the corroded solder joints at 24 h. However, corrosion products on the solder joint begin to accumulate and grow. Gradually, additional flake corrosion products are formed, increasing the number of rose petals. In summary, the corrosion of solder joints becomes more severe with increasing corrosion time, exhibiting an increasing trend in the diameter of solder joints.

3.2 Electrical performance degradation

Figure 6 displays the degradation paths of board-level components at disparate temperatures. In the same experiment, three identical board-level components are introduced simultaneously. The degradation paths of three identical board-level components are labeled as S1, S2 and S3, respectively. It can be observed from Fig. 6 that

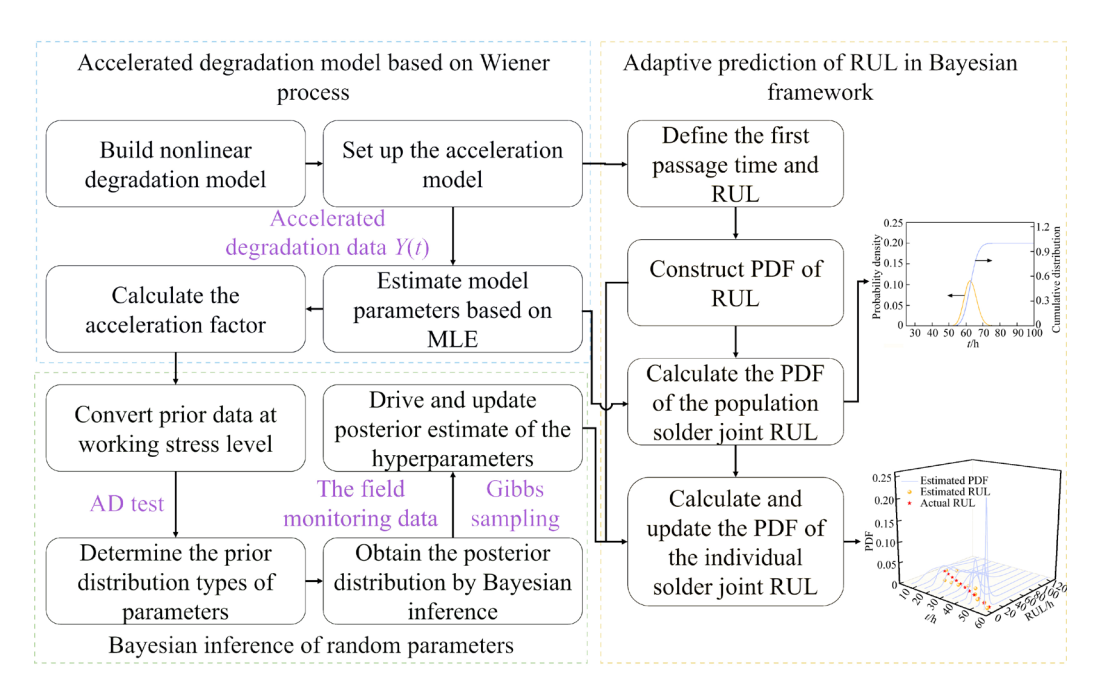


Fig. 4 Flow chart of RUL prediction in Bayesian framework

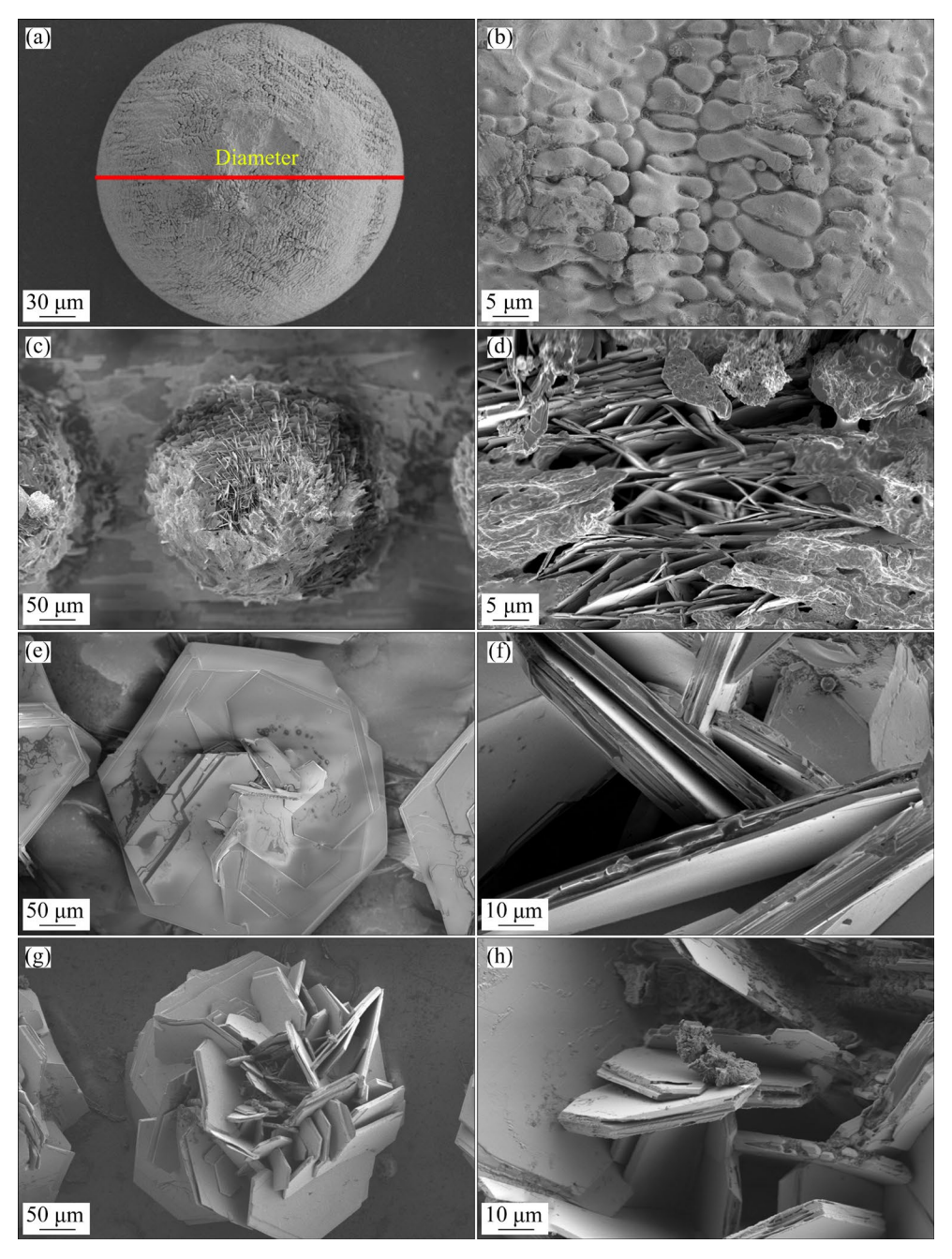


Fig. 5 Corrosion morphology of solder joints in PVC fire smoke at different time: (a, b) 0 h; (c, d) 3 h; (e, f) 24 h; (g, h) 48 h

under all temperature stresses, the RCR of board-level components shows a nonlinear increasing trend. This observation corresponds to the corrosion morphology of solder joints depicted in Fig. 5. It is attributed to the corrosive effect of PVC smoke on the electrical connection points of board-level components, namely the solder joint, which leads to numerous voids within the solder joints. The solder joints change from a spherical shape with a tight structure to a rose shape with many voids and loose sheet corrosion products.

In this process, the cross-sectional area of the solder joint decreases. The solder joint material used in the experiment is SAC305, which is constant. Due to the packaging of the board-level components, the solder joint height has also been fixed. In other words, the solder joint resistivity (ρ) and the current flow length (L) are unchanged. According to the resistance calculation formula $R=(\rho L)/A$, the reduction in the cross-sectional area (A) of the solder joint results in an increase in resistance (R).

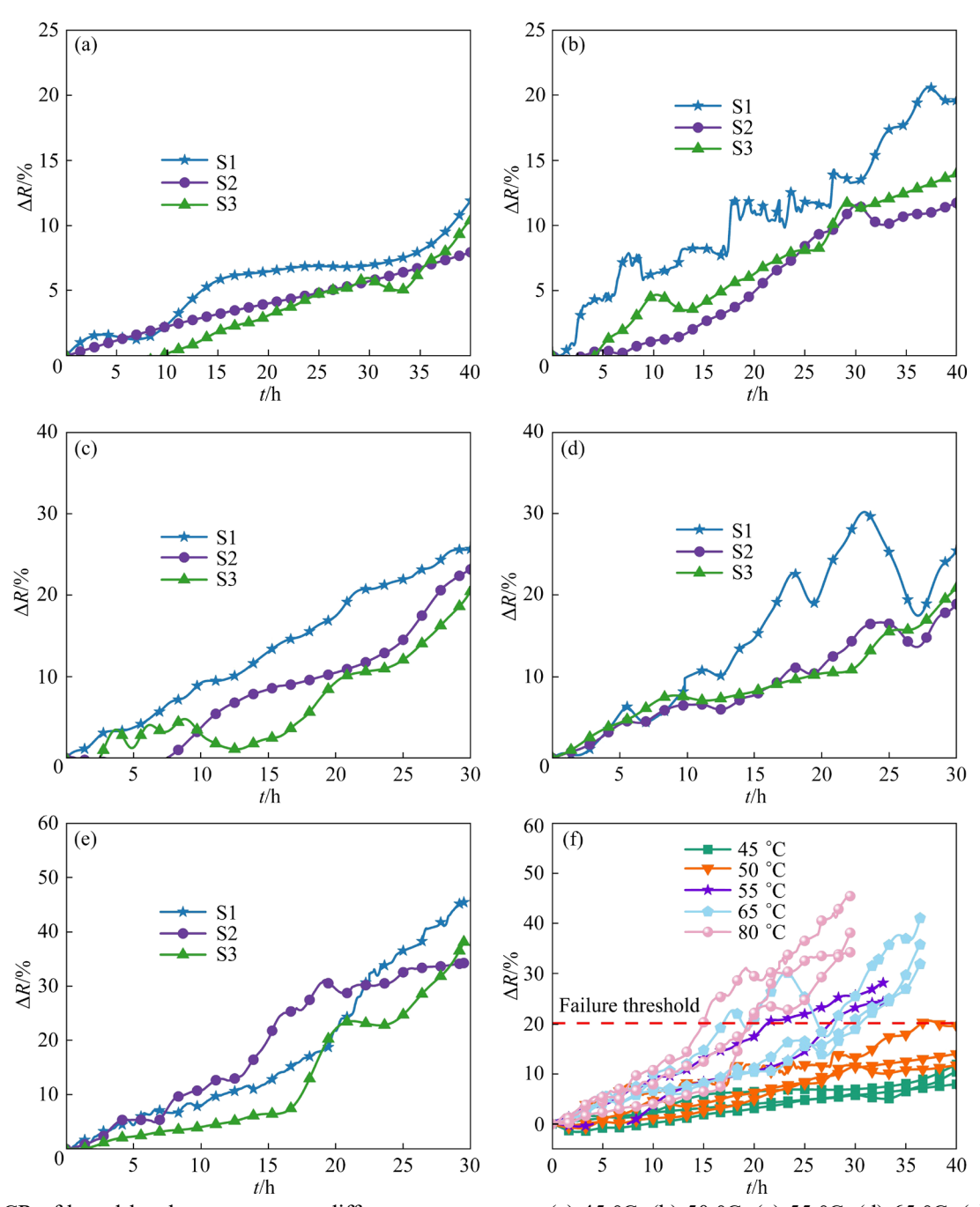


Fig. 6 RCR of board-level components at different temperatures: (a) 45 °C; (b) 50 °C; (c) 55 °C; (d) 65 °C; (e) 80 °C; (f) Comparison at different temperatures

To better demonstrate the experimental repeatability, the degradation paths of board-level components at different temperatures are compared in Fig. 6(f). Due to the strict control and maintenance of the experimental setup and conditions, certain regularities in the degradation paths of board-level components at different temperatures can be identified. With increasing temperature, the degradation rate of the board-level components accelerates. However, the degradation paths of all board-level components under the same

temperature conditions generally fall within a defined range. The above phenomena confirm the feasibility of the experiment and the reproducibility of the results. Nevertheless, it can be observed from Fig. 6(f) that the degradation paths of board-level components at the same temperature are not completely consistent and show individual variations.

It can be observed from Fig. 6 that the resistance increase rate varies at different temperatures. Higher temperatures accelerate the

corrosion of the solder joints, resulting in a faster increase in the resistance of board-level components. In Fig. 7, the logarithm form of the Arrhenius equation is used to describe the relationship between solder joints FT and temperature stress. The Arrhenius equation and its logarithmic form are shown in Eqs. (18) and (19). It can be found that the points at all temperature levels are within the 80% confidence band, indicating that the Arrhenius equation can well fit the relationship between temperature and FT. The feasibility of using the Arrhenius equation to establish the accelerated degradation model is confirmed.

$$t = A \exp\left(\frac{E_{\rm a}}{k_{\rm B}T}\right) \tag{18}$$

$$\ln t = \ln A + (E_{\rm a}/k_{\rm B}) \cdot (1/T) \tag{19}$$

where t is FT, h; A is the constant of the model; E_a is the activation energy of electrochemical corrosion, eV; k_B is the Boltzmann constant; T is the temperature, K.

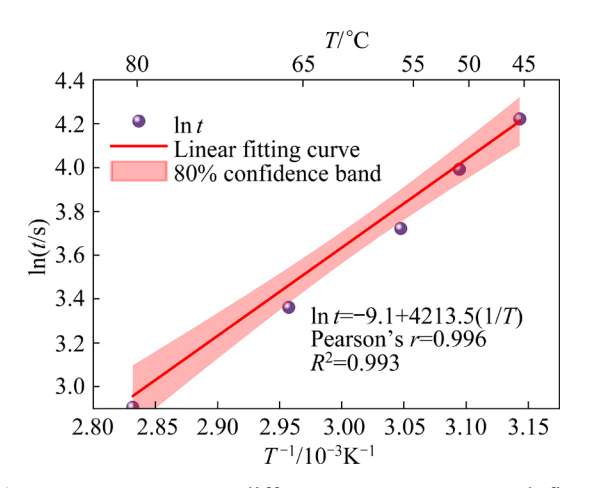


Fig. 7 Average FT at different temperatures and fitted curve

3.3 Average life prediction

To validate the effectiveness of the proposed life prediction model (Eq. (9)), the experimental data at 45 °C were used as historical data. The life of the solder joints at 45 °C in the smoke environment is predicted using the historical data and compared with the experimental values. The parameter estimates of the proposed model can be obtained by analyzing single board-level components at each stress level, as summarized in Table 1. With the increase of the temperature stress, the drift and diffusion coefficients present a rising trend, which is consistent with the law of accelerated degradation of board-level components under high temperature stress. Despite the occasional abnormal behavior of the individual board-level components, the parameter estimates at high temperature stress levels are lower than those at low stress levels, which is attributed to experimental errors. However, the overall variation trend remains unaffected, and subsequent parameter estimation and calculation will not be affected.

Table 1 Parameter estimate for each board-level component at different temperatures

Temperature/	S1		S2		S3	
°C	μ /	σ^{2}	μ /	σ^2 /	μ	σ^2 /
	10^{-3}	10^{-2}	10^{-3}	10^{-2}	10^{-3}	10^{-2}
50	3.44	0.93	4.00	0.47	4.38	1.20
55	6.10	2.05	12.87	0.75	8.23	1.67
65	1.59	23.51	12.14	1.18	15.46	5.52
80	1.80	36.19	10.22	4.86	13.59	54.64

The two-step estimation method is employed to estimate the overall parameters of the accelerated degradation model. The final overall parameter estimates are obtained as follows:

$$(\hat{a}_{1}^{*}, \hat{c}_{1}^{*}, \hat{a}_{2}^{*}, \hat{\beta}^{*}) = [5.40, 3371.51, -0.56, 0.95]$$

By performing calculations, the estimated values of the model parameters are shown in Table 2, and the predicted average life of the board-level component at 45 °C is obtained. Subsequently, by substituting the estimated parameters into Eqs. (7) and (8), the PDF and CDF of the average life of board-level components can be obtained, as schematically illustrated in Fig. 8.

Table 2 Parameter estimate and average life at 45 °C

Parameter	Estimation		
μ	3.17×10^{-3}		
σ^2	2.41×10^{-6}		
Average life	66.16		

Three board-level components are tested at 45 °C. The average value of RCR is obtained, and the average degradation path is presented in Fig. 9. The degradation path reaches the failure threshold for the first time at 68.91 h and 45 °C, indicating that the actual life of board-level components is 68.91 h. Based on the experimental dataset of the

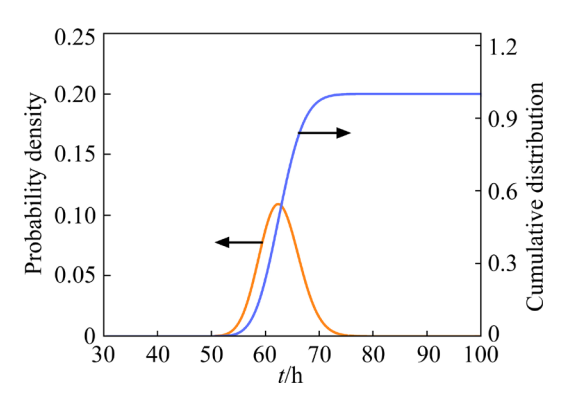


Fig. 8 PDF and CDF of average life of board-level components at 45 °C

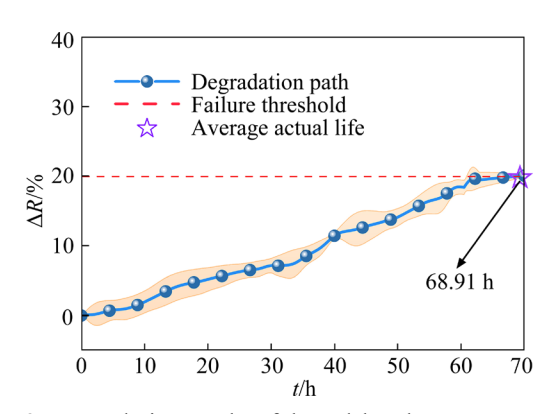


Fig. 9 Degradation path of board-level components at $45\,^{\circ}\mathrm{C}$

board-level component at other temperature levels, the average life of the board-level components at 45 °C is determined to be 66.16 h. Therefore, the relative error of the prediction result is approximately 4%, indicating a relatively low error level. The comparison results demonstrate that the solder joint life prediction model constructed with the nonlinear Wiener process and Arrhenius equation exhibits high accuracy and can accurately predict the average life of solder joints after corrosion.

3.4 Adaptive RUL prediction

Based on the calculation method described in Eq. (14), the temperature-related model parameters in Table 1 are transformed into model parameter values at 45 °C, as shown in Table 3.

Since normal distribution, gamma distribution, lognormal distribution, Weibull distribution, extreme value distribution, and exponential distribution cover most of the distribution of parameters, these six distributions are selected as the feasible distribution types of random parameters. The results of the AD test are schematized in Table 4.

Table 3 Parameter estimate for each solder joint corresponding to conversion to operating temperature stress level

Temperature/-	S1		S2		S3	
°C	$\mu/10^{-3}$	$\sigma^{2/}$ 10^{-2}	μ/ 10 ⁻³	$\frac{\sigma^{2}}{10^{-2}}$	$\frac{\mu}{10^{-3}}$	$\frac{\sigma^{2}}{10^{-2}}$
50	2.94	0.80	3.42		3.75	1.43
55	6.05	4.06	9.46	3.57	11.71	1.51
65	3.34	12.94	6.68	0.41	8.51	30.06
80	6.62	13.30	3.75	0.17	4.99	0.44

A smaller value of the AD test indicates a closer fit of the data distribution to the target distribution. Consequently, it can be concluded from Table 3 that the optimal fitting prior distribution for μ and σ^2 is determined separately as the normal distribution and Weibull distribution.

Figure 10 illustrates the degradation path of individual board-level components at 45 °C, and the corresponding actual life is approximately 64.22 h when the RCR reaches the failure threshold for the first time.

Whenever new monitoring data become available, the Bayesian method iteratively updates the posterior estimates of the random parameters. As a result, the new adaptive RUL estimates and their PDFs are updated automatically. Figure 11 depicts the PDFs of RUL at different time. It is evident that as on-site monitoring data are continuously updated and accumulated, the peak PDF value of RUL increases, indicating that the prediction accuracy of the model gradually improves and the uncertainty of the model decreases. The improved prediction accuracy is attributed to using

Table 4 AD statistics results of μ and σ^2 under various distribution types

Parameter	Normal	Gamma	Lognormal	Weibull	Extreme value	Exponential
μ	1.54	16.27	16.27	57.62	1.84	16.27
σ^2	1.39	1.41	7.27	1.11	1.78	7.27

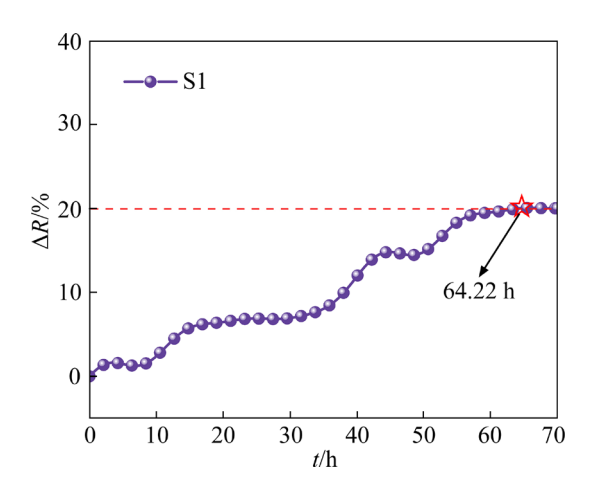


Fig. 10 Degradation path of RCR of individual board-level component at 45 °C

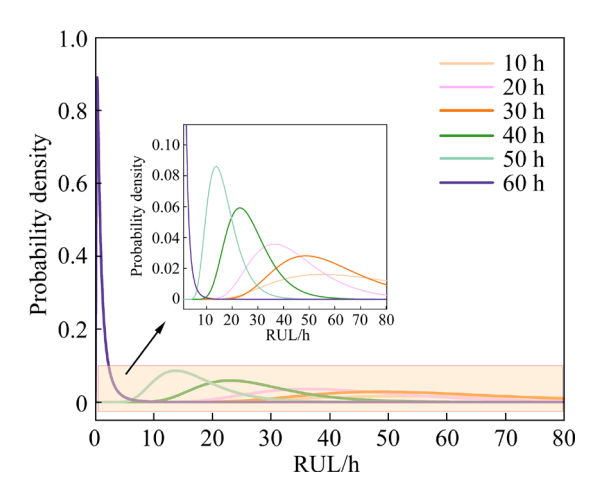


Fig. 11 PDF of RUL for individual board-level component

an adaptive estimation scheme. The scheme takes advantage of the growing amount of data to refine the parameter estimation, thereby mitigating the uncertainty associated with the parameter estimation. This reveals that the proposed model has perfect adaptability.

To assess the reliability of the proposed model in predicting the RUL, confidence intervals are utilized to quantify the model's performance. Figure 12 displays the actual and estimated RUL of individual board-level component at different time and the ±20% confidence interval corresponding to the actual values. The red line represents the actual RUL, and the orange line represents the estimated RUL. The solid green lines represent the upper and lower limits of the 20% forecast deviation allowed by the actual RUL, respectively. The green shaded areas represent the corresponding forecast deviation ranges. Although the prediction error is large at the

beginning stage, the predicted RUL can fall within the confidence interval at the late stage of the degradation path. The results show that the method is adaptable, and with the accumulation of monitoring data, the accuracy of the prediction will be improved. Moreover, the proposed method is effective and robust for predicting the RUL of individual solder joints.

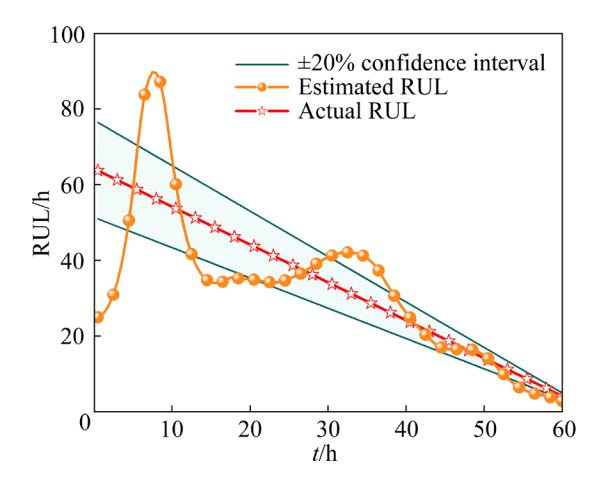


Fig. 12 Comparison of actual RUL and estimated RUL

To further assess the predictive accuracy and effectiveness of the proposed RUL prediction models, two evaluation metrics, namely the absolute error (AE) and mean square error (MSE), are employed, as presented in Eqs. (20) and (21). These metrics provide a quantitative measure of difference between the predicted and actual RUL values, thus serving as objective measures of model performance. Precisely, the AE measures the difference between predicted and actual RUL values, while the MSE reflects the average squared difference between predicted and actual RUL values. Lower AE and MSE values indicate higher prediction accuracy of the model.

$$\varepsilon_{AE} = \overline{\xi}_{RUL_i} - \xi_{RUL_i} \tag{20}$$

$$\varepsilon_{\text{MSE}} = \frac{1}{n} \sum_{i=1}^{n} \left(\overline{\xi}_{\text{RUL}_i} - \xi_{\text{RUL}_i} \right)^2$$
 (21)

where ξ_{RUL_i} (h) is the actual value of RUL at the moment of t_i , and $\overline{\xi}_{\text{RUL}_i}$ (h) is the predicted value of RUL at the moment of t_i .

The AE and MSE of RUL are plotted in Fig. 13. It can be seen that the AE descends to a certain extent with the increase of the field observed data, indicating that the length of the observation history will affect the parameter estimation. In

addition, the AE is controlled within 20% and is close to 0 in the later degradation period. Similarly, the MSE tends to be 0 overall. The comparison results with experimental data indicate that the model exhibits high prediction accuracy and can be used to predict the RUL of solder joints after corrosion.

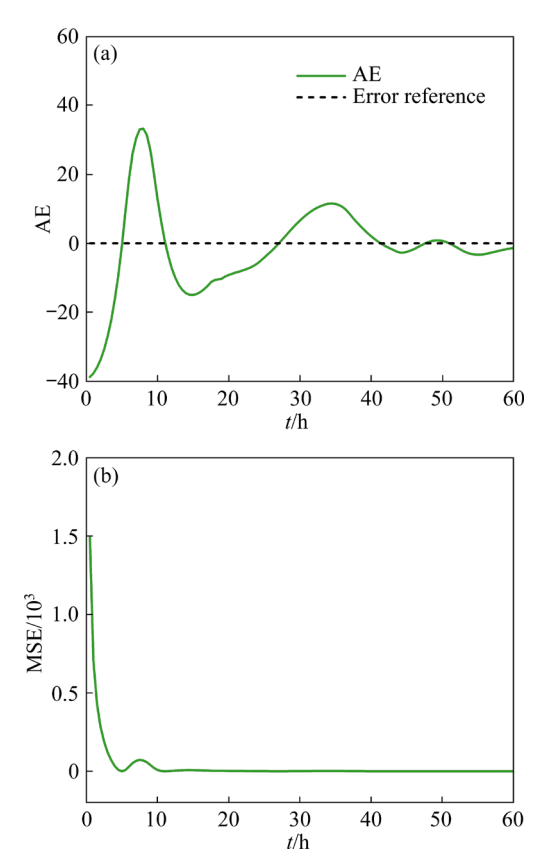


Fig. 13 AE (a) and MSE (b) of RUL

Based on the above research results, the proposed model is adaptable, robust, and has lower uncertainty. In particular, it can predict the RUL of solder joints well. Meanwhile, with the accumulation of field monitoring data, the uncertainty of parameter estimation gradually declines, which implies the feasibility of achieving adaptive estimation of the RUL for solder joints within the Bayesian framework.

4 Conclusions

(1) The corrosion of solder joints is evident in the early smoke exposure stage. Numerous corrosion pits are observed on the surface of the solder joints, and the overall shape of the solder joints resembles a prickly sphere. Over time, the solder joints transform from a spherical shape to a blooming rose shape, and the corrosion products change from dense thin layers to loose thick layers.

- (2) The degradation of solder joints' electrical performance is closely related to surface corrosion. The surface corrosion reduces the cross-sectional area and increases the resistance of the solder joints, which eventually leads to failure. Individual variations exist in the degradation paths of different board-level components at the same temperature. An increase in temperature accelerates the degradation rate of board-level components.
- (3) Average life and RUL prediction models for solder joints in the fire smoke environment are established. The predicted average life from the established life prediction model is 66.16 h, with a relative error of 4% compared to the experimental value of 68.9h. The accuracy of the average life prediction model is verified. Furthermore, with new monitoring data, the proposed RUL prediction framework based on Bayesian method successfully estimated updates the random parameters, achieving adaptive and accurate predictions for the RUL.

CRediT authorship contribution statement

Meng-ke ZHAO: Investigation, Methodology, Validation, Formal analysis, Writing — Original draft; Jian-rui FENG: Data curation, Visualization; Qian LI: Conceptualization, Project administration, Writing — Review & editing; Shou-xiang LU: Resources, Supervision, Writing — Review & editing; Jin LIN: Funding acquisition.

Declaration of competing interest

The authors declare that they have no known competing financial interests or personal relationships that could have appeared to influence the work reported in this paper.

Data availability statement

The raw data related to this manuscript will be made available upon request.

Acknowledgments

This work was financially supported by the National Natural Science Foundation of China (No. 52206180), and the Fundamental Research Funds for the Central Universities, China (No. WK2320000050).

Supporting Information

Supporting Information in this paper can be found http://tnmsc.csu.edu.cn/download/15-p0538-2023-

0750-Supporting Information.pdf.

References

- [1] CHANTARAMANEE S, SUNGKHAPHAITOON P. Combined effects of Bi and Sb elements on microstructure, thermal and mechanical properties of Sn-0.7Ag-0.5Cu solder alloys [J]. Transactions of Nonferrous Metals Society of China, 2022, 32: 3301-3311.
- [2] HAN Yong-dian, YANG Jia-hang, XU Lian-yong, JING Hong-yang, ZHAO Lei. Effect of transient current bonding on interfacial reaction in Ag-coated graphene Sn-Ag-Cu composite solder joints [J]. Transactions of Nonferrous Metals Society of China, 2021, 31: 2454–2467.
- [3] CHANTARAMANEE S, SUNGKHAPHAITOON P. Influence of bismuth on microstructure, thermal properties, mechanical performance, and interfacial behavior of SAC_{305-x}Bi/Cu solder joints [J]. Transactions of Nonferrous Metals Society of China, 2021, 31: 1397–1410.
- [4] WANG Ming-na, WANG Jian-qiu, KE Wei. Corrosion behavior of Sn-3.0Ag-0.5Cu solder under high-temperature and high-humidity condition [J]. Journal of Materials Science: Materials in Electronics, 2014, 25: 1228-1236.
- [5] HUANG Ming-liang, ZHAO Ning, LIU Shuang, HE Yi-qian. Drop failure modes of Sn-3.0Ag-0.5Cu solder joints in wafer level chip scale package [J]. Transactions of Nonferrous Metals Society of China, 2016, 26: 1663-1669.
- [6] FENG Jian-rui, ZHAO Meng-ke, LU Shou-xiang. Accident spread and risk propagation mechanism in complex industrial system network [J]. Reliability Engineering & System Safety, 2024, 244: 109940.
- [7] LI Qian, LIN Jin, LI Chang-hai, LU Shou-xiang, CHEN Xiao. Effect of polyvinyl chloride fire smoke on the long-term corrosion kinetics and surface microstructure of tin–lead and lead-free solders [J]. Journal of Materials Science: Materials in Electronics, 2019, 30: 16395–16406.
- [8] LI Qian, LIN Jin, LI Chang-hai, LU Shou-xiang, CHEN Xiao. Effect of relative humidity on corrosion behavior of SAC305 and Sn-37Pb solders under polyvinyl chloride fire smoke atmosphere [J]. Journal of Materials Science: Materials in Electronics, 2020, 31: 19920-19930.
- [9] LI Qian, LIN Jin, LI Chang-hai, LU Shou-xiang, CHEN Xiao. Effect of relative humidity on the corrosion behavior of Sn-0.7Cu solder under polyvinyl chloride fire smoke atmosphere [J]. Materials and Corrosion, 2020, 71: 1729-1735.
- [10] LIAO Bo-kai, CEN Hong-yu, CHEN Zhen-yu, GUO Xing-peng. Corrosion behavior of Sn-3.0Ag-0.5Cu alloy under chlorine-containing thin electrolyte layers [J]. Corrosion Science, 2018, 143: 347-361.
- [11] QIAO Chuang, WANG Ming-na, HAO Long, LIU Xia-he, JIANG Xiao-lin, AN Xi-zhong, LI Duan-yang. Temperature and NaCl deposition dependent corrosion of SAC305 solder alloy in simulated marine atmosphere [J]. Journal of Materials Science & Technology, 2021, 75: 252–264.
- [12] MOHANTY U S, LIN K L. Electrochemical corrosion study of Sn-xAg-0.5Cu alloys in 3.5% NaCl solution [J]. Journal of Materials Research, 2007, 22: 2573–2581.

- [13] OSÓRIO W R, LEIVA D R, PEIXOTO L C, GARCIA L R, GARCIA A. Mechanical properties of Sn-Ag lead-free solder alloys based on the dendritic array and Ag₃Sn morphology [J]. Journal of Alloys and Compounds, 2013, 562: 194-204.
- [14] ZHANG Hui-zhe, MA Zhao-long, YANG Su-yuan, FAN Meng-zhuo, CHENG Xing-wang. Microstructure and mechanical properties of Sn-xGa alloys and solder joints [J]. Journal of Materials Research and Technology, 2023, 26: 3830–3839.
- [15] CHEN Wen-jing, YE Nan, ZHUO Hai-ou, TANG Jian-cheng. Electrochemical corrosion behaviour of Zn-Sn-Cu-xNi lead-free solder alloys [J]. Transactions of Nonferrous Metals Society of China, 2023, 33: 2740–2750.
- [16] TUNTHAWIROON P, KANLAYASIRI K. Effects of Ag contents in Sn-xAg lead-free solders on microstructure, corrosion behavior and interfacial reaction with Cu substrate [J]. Transactions of Nonferrous Metals Society of China, 2019, 29: 1696–1704.
- [17] SATIZABAL L M, COSTA D, MORAES P B, BORTOLOZO A D, OSÓRIO W R. Microstructural array and solute content affecting electrochemical behavior of Sn-Ag and Sn-Bi alloys compared with a traditional Sn-Pb alloy [J]. Materials Chemistry and Physics, 2019, 223: 410-425.
- [18] GUÉDON-GRACIA A, FRÉMONT H, PLANO B, DELÉTAGE J Y, WEIDE-ZAAGE K. Effects of salt spray test on lead-free solder alloy [J]. Microelectronics Reliability, 2016, 64: 242–247.
- [19] GAO Yan-fang, CHENG Cong-qian, ZHAO Jie, WANG Li-hua, LI Xiao-gang. Electrochemical corrosion of Sn-0.75Cu solder joints in NaCl solution [J]. Transactions of Nonferrous Metals Society of China, 2012, 22: 977-982.
- [20] WANG Ming-na, WANG Jian-qiu, KE Wei. Corrosion behavior of Sn-3.0Ag-0.5Cu lead-free solder joints [J]. Microelectronics Reliability, 2017, 73: 69-75.
- [21] CHEN Yao-jun, JING Bo, LI Jian-feng, JIAO Xiao-xuan, HU Jia-xing, WANG Yun. Failure analysis and modeling of solder joints in BGA packaged electronic chips [J]. IEEE Transactions on Components, Packaging and Manufacturing Technology, 2020, 11: 43–50.
- [22] LIU Bo, LEE T K, LIU Kuo-chuan. Impact of 5% NaCl salt spray pretreatment on the long-term reliability of wafer-level packages with Sn-Pb and Sn-Ag-Cu solder interconnects [J]. Journal of Electronic Materials, 2011, 40: 2111–2118.
- [23] RAMAKRISHNAN A, PECHT M G. A life consumption monitoring methodology for electronic systems [J]. IEEE Transactions on Components and Packaging technologies, 2003, 26: 625-634.
- [24] WANG Zhi-hua, LI Jun-xing, MA Xiao-bing, ZHANG Yong-bo, FU Hui-min, KRISHNASWAMY S. A generalized Wiener process degradation model with two transformed time scales [J]. Quality and Reliability Engineering International, 2017, 33: 693-708.
- [25] QIAO Chuang, WANG Ming-na, HAO Long, JIANG Xiao-lin, LIU Xia-he, THEE C, AN Xi-zhong. In-situ EIS study on the initial corrosion evolution behavior of SAC305 solder alloy covered with NaCl solution [J]. Journal of

- Alloys and Compounds, 2021, 852: 156953.
- [26] SI Xiao-sheng, WANG Wen-bin, HU Chang-hua, ZHOU Dong-hua, PECHT M G. Remaining useful life estimation based on a nonlinear diffusion degradation process [J]. IEEE Transactions on Reliability, 2012, 61: 50–67.
- [27] PANG Zhe-nan, SI Xiao-sheng, HU Chang-hua, DU Dang-bo, PEI Hong. A Bayesian inference for remaining useful life estimation by fusing accelerated degradation data and condition monitoring data [J]. Reliability Engineering & System Safety, 2021, 208: 107341.
- [28] AKODA K E, GUEDON-GRACIA A, DELETAGE J Y,

- PLANO B, FREMONT H. Impact of temperature on the corrosion of lead-free solder alloy during salt spray test [J]. Microelectronics Reliability, 2021, 126: 114286.
- [29] WHITMORE G A, SCHENKELBERG F. Modelling accelerated degradation data using Wiener diffusion with a time scale transformation [J]. Lifetime Data Analysis, 1997, 3: 27–45.
- [30] SI Xiao-sheng, WANG Wen-bin, HU Chang-hua, ZHOU Dong-hua. Remaining useful life estimation—A review on the statistical data driven approaches [J]. European Journal of Operational Research, 2011, 213: 1–14.

SAC305 焊点在聚氯乙烯火灾烟气中的腐蚀行为及寿命预测

赵梦珂, 冯舰锐, 李倩, 陆守香, 林锦

中国科学技术大学 火灾安全全国重点实验室, 合肥 230026

摘 要: 开展烟雾暴露实验研究 Sn-3.0Ag-0.5Cu 焊点在 45~80 ℃温度范围内的腐蚀行为和寿命。利用非线性 Wiener 过程和 Arrhenius 方程建立焊点平均寿命和个体剩余使用寿命的概率分布函数和预测模型。结果表明,随 着时间的增加,焊点电阻呈非线性增长趋势。24 小时后,焊点由球形转变为玫瑰形。温度越高,焊点失效越快,失效时间与温度的关系符合 Arrhenius 方程。模型预测寿命与实验结果吻合较好,验证了模型的有效性和准确性。 关键词: 焊点; 火灾烟雾; 腐蚀行为; 电性能退化; 寿命预测模型

(Edited by Xiang-qun LI)